ACS APPLIED MATERIALS & INTERFACES

Research Article

www.acsami.org

Fabrication of Polymer Nanocapsules with Controllable Oligo(Ethylene Glycol) Densities, Permeation Properties and Robustly Crosslinked Walls

Tianyou Chen, Binyang Du,* Xinghong Zhang, and Zhiqiang Fan

MOE Key Laboratory of Macromolecular Synthesis and Functionalization, Department of Polymer Science & Engineering, Zhejiang University, Hangzhou 310027, China

Supporting Information

ABSTRACT: P(TMSPMA-*co*-OEGMA) nanocapsules with controllable oligo(ethylene glycol) (OEG) densities and robustly cross-linked structures were successfully fabricated from the cross-linkable copolymer, poly[3-(trimethoxysilyl)propyl methacrylate-*co*-oligo(ethylene glycol) methacrylate] (P(TMSPMA-*co*-OEGMA)). The densities of OEG segments of the resultant P(TMSPMA-*co*-OEGMA) nanocapsules could be easily controlled by tuning the OEGMA contents of copolymer P(TMSPMA-*co*-OEGMA). The microenvironments of the P(TMSPMA-*co*-OEGMA) nanocapsules were determined to be hydrophobic. It was demonstrated that hydrophobic pyrene could be in situ loaded into the P(TMSPMA-*co*-OEGMA) nanocapsules during the fabrication procedure. The release rates of pyrene from the P(TMSPMA-*co*-OEGMA) nanocapsules were dependent on the contents of OEGMA, indicating that the permeation properties of P(TMSPMA-*co*-OEGMA) nanocapsules could be tuned by varying the cross-linked densities of the nanocapsule walls. It was further demonstrated that other functional groups could be easily incorporated into the resultant polymer nanocapsules by using the similar procedure. The preparation of polymer nanocapsules with various functionalities and robustly cross-linked walls without any further post modification process, any sacrificial core and surfactant would be beneficial from scientific and technical point of views.

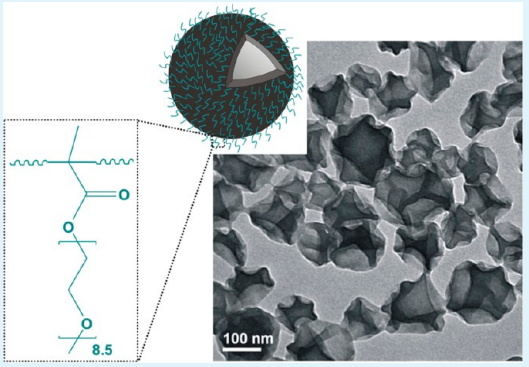

KEYWORDS: *polymer nanocapsules, oligo(ethylene glycol) densities, cross-linked walls, permeation properties, controllable*

1. INTRODUCTION

Polymer nanocapsules, which have very thin polymer shells but large rooms for the encapsulation and release of various kinds of species, such as drug,[1] contrast agent,[2] protein,[3] RNA,[4] and DNA,[5] are nanoparticles with hollow structures. There are many potential applications for polymer nanocapsules in the fields of drug delivery,[6] catalysis,[7] cancer therapy,[8] and protecting enzymes.[9] In recent decades, various methods have been developed for the preparation of polymer nanocapsules, including layer-by-layer assembly,[9−11] double emulsions,[12−14] polymer precipitation by phase separation,[15] microemulsion polymerization,[16] polymer growth by a surface polymerization,[17] vesicles assemble by amphiphilic copolymers,[18,19] polymerization of hydrophobic monomers in lipid bilayer templates,[20−22] and among others. However, most of these methods needed an extra process to remove the solid cores or surfactants, which were used during the fabrication of polymer nanocapsules, for further applications.[9,16,17,22] Furthermore, most of the obtained polymer micro or nanocapsules were not fixed by chemical cross-linking and easy to deform or decompose under the environmental change. To preserve the structural integrity of polymer nanocapsules under varying conditions, the cross-linking would be the key step to fabricate stable and robust nanocapsules. By choosing a reactive function monomer, 3-(trimethoxysilyl)propyl methacrylate (TMSPMA), our group reported recently the successful fabrication of robust and cross-linked polymer nanocapsules from the cross-linkable polymer, poly[3-(trimethoxysilyl)propyl methacrylate] (PTMSPMA), in an oil-in-water emulsion by utilizing the hydrolysis and condensation of methoxysilyl groups.[23] PTMSPMA has been used for the preparation of organic−inorganic hybrid materials, like nanotubes, capsules, and microgels, etc.[19,24−28] Such polymer nanocapsules with robustly cross-linked structures might find potential applications for the encapsulations of catalysts, dyes, drugs, etc.

The prospective applications of polymer nanocapsules, for instance, as drug delivery systems, usually require surface modifications of the nanocapsules, which could help to improve the in vivo stabilities of the nanocapsules and to avoid uptakes of the nanocapsules by the reticular endothelial system.[29−31] Two main types of methods have been reported for the preparation of polymer nanocapsules with modified surfaces,

Received: January 27, 2013
Accepted: April 9, 2013
Published: April 9, 2013

   dx.doi.org/10.1021/am400365s | ACS Appl. Mater. Interfaces 2013, 5, 3748−3756

Scheme 1. Schematic of Free Radical Copolymerization of TMSPMA and OEGMA, and the Hydrolysis and Condensation Reactions of Methoxysilyl Groups of P(TMSPMA-*co*-OEGMA)

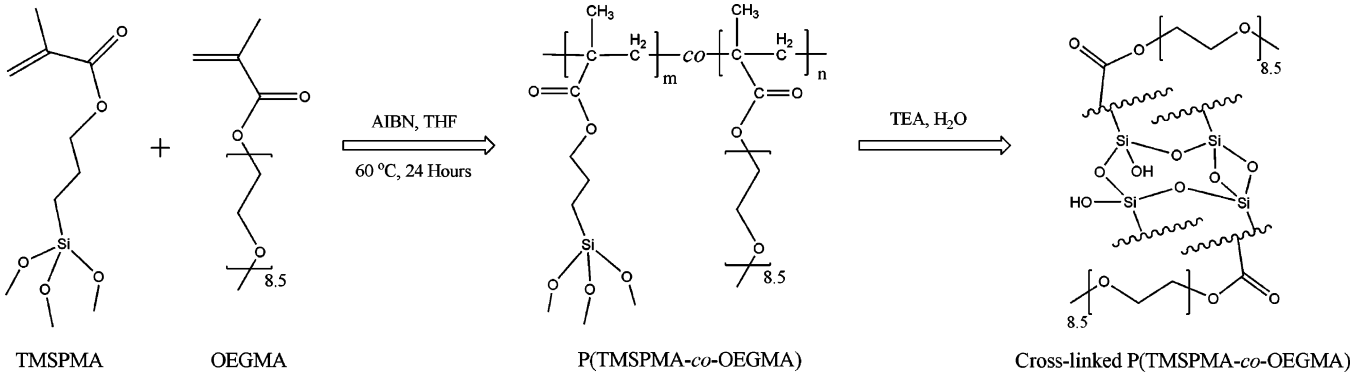

that is, grafting-to method and grafting-from method. The grafting-to method, like surface electrostatic adsorption[31] and surface click reaction,[11,32] was most extensively used for the surface modification of polymer nanocapsules. However, it was usually costly and time-consuming. Furthermore, it was less controllable for grafting-to method to modify the polymer nanocapsules because the surface densities of functional groups of the polymer nanocapsules were largely influenced by chain conformation, which relied on solvent, concentration, molecular weight, temperature, etc.[30] The grafting-from method, including self-assembly of block copolymer,[18,19] polymerization of hydrophobic monomers in lipid bilayer templates[20−22] and interfacial polyaddition,[33,34] could be the good choice for the preparation of polymer nanocapsules with surface modification in one step. However, neither polymerization of hydrophobic monomers in lipid bilayer templates nor self-assembly of block copolymer could control the surface densities of functional groups of the resultant polymer nanocapsules. Small molecules (e.g., lipid egg phosphatidylcholine)[22] and macromolecules (e.g., poly(ethylene glycol) (PEG))[2,30,33,35] were usually chosen for the surface modification of nanocapsules or nanoparticles. Undoubtedly, PEG was the most widely preferred choice for the surface modification of nanocapsules and nanoparticles. PEG is highly hydrophilic, nontoxic, and has very low level of protein or cellular adsorption.[36,37] It was found that the PEG density on the nanoparticle surfaces was a critical factor for modulating nanoparticle circulation time[38] and nonspecific cellular uptake.[39] Recently, Morral-Ruíz et al. reported the preparation of PEGylated polyurethane nanocapsules via interfacial polyaddition.[33] However, side reactions, which may influence the surface density of PEG, could not be avoided.[33] Furthermore, the monomer isophorone diisocyanate was also too reactivity and might react with incorporation species.[33] Therefore, in spite of intensive efforts, it is still a challenge to prepare polymer nanocapsules with precise control of surface functionality and functional density without side reactions.

In the present work, we reported the facile fabrication of polymer nanocapsules with precise control of oligo(ethylene glycol) (OEG) densities and robustly cross-linked structures from the cross-linkable copolymer, poly[3-(trimethoxysilyl)-propyl methacrylate-*co*-oligo(ethylene glycol) methacrylate] (P(TMSPMA-*co*-OEGMA)). Linear cross-linkable copolymers P(TMSPMA-*co*-OEGMA)s were first synthesized by free radical copolymerization of monomers TMSPMA and OEGMA and then applied for the fabrication of P-(TMSPMA-*co*-OEGMA) nanocapsules using the similar method that we developed previously.[23] The densities of OEG segments of the resultant P(TMSPMA-*co*-OEGMA) nanocapsules could be easily controlled by tuning the OEGMA contents of P(TMSPMA-*co*-OEGMA). Furthermore, the contents of OEG segments were already fixed during copolymerization and would not be affected during the fabrication process of polymer nanocapsules. It was found that the OEGMA contents of P(TMSPMA-*co*-OEGMA) copolymers determined the successful fabrication of the nanocapsules, which could be only obtained in a certain range of OEGMA contents. We demonstrated that hydrophobic pyrene could be in situ loaded into the P(TMSPMA-*co*-OEGMA) nanocapsules during the fabrication procedure. The release rates of pyrene from the P(TMSPMA-*co*-OEGMA) nanocapsules were dependent on the contents of OEGMA, which indicated that the permeation properties of P-(TMSPMA-*co*-OEGMA) nanocapsules could be also controlled by varying the cross-linked densities of the walls of the nanocapsules. We also demonstrated that such methodology could be applied to incorporate other functional groups into the polymer nanocapsules.

2. EXPERIMENTAL SECTION

2.1. Chemicals and Materials. 3-(Trimethoxysilyl)propyl methacrylate (TMSPMA, 98%) and pyrene (98%) were purchased from Acros Organics and used as received. Oligo(ethylene glycol) methacrylate (OEGMA, M_n = 475) was purchased from Sigma-Aldrich and used without further purification. α,α'-Azodiisobutyronitrile (AIBN, Sinopharm Chemical Reagent Co., Ltd.) was recrystallized from methanol and dried under vacuum at room temperature for 24 h to remove methanol. Anhydrous tetrahydrofuran (THF, Sinopharm Chemical Reagent Co., Ltd.) was dried by refluxing in the presence of a sodium flake and distilled prior to use. All other reagents were of analytical grade and used as received. Deionized water was used throughout the experiments.

2.2. Synthesis of Poly[3-(trimethoxysilyl)propyl methacrylate-*co*-oligo(ethylene glycol) methacrylate] (P(TMSPMA-*co*-OEGMA)) Copolymers. A series of P(TMSPMA-*co*-OEGMA) copolymers were synthesized by free radical copolymerization of TMSPMA and various amounts of OEGMA. The chemical structures of TMSPMA, OEGMA and copolymer P(TMSPMA-*co*-OEGMA) were shown in Scheme 1. Typically, 15 mg of AIBN, 0.50 mL of TMSPMA, and various amounts of OEGMA were dissolved in 5 mL of anhydrous THF with gently magnetic stirring. The solution was then bubbled with nitrogen for 30 min to eliminate the oxygen. The copolymerization was initiated by rising the temperature of the solution to 60 °C and allowed to proceed for 24 h. The resultant copolymers were precipitated from *n*-hexane and washed for three times. The precipitates were collected and dried under vacuum at 30

°C for 24 h. Finally, colorless and grease-like products were obtained and stored in a vacuum desiccator for further uses.

The ^{1}H NMR spectra of the obtained P(TMSPMA-*co*-OEGMA) copolymers are shown in Figure S1 (see Supporting Information). The characteristic signals at 3.5−3.6 ppm and 3.6−3.7 ppm are assigned to the $[-Si(OCH_3)_3]$ groups of TMSPMA and the $[-(CH_2)_2O-]$ groups of OEGMA, respectively, indicating the successful copolymerization of TMSPMA and OEGMA. The contents of OEGMA of the copolymers could be determined from their ^{1}H NMR spectra. The number-average molecular weights (M_n) and the polydispersity indices (PDI, M_w/M_n) of the copolymers were determined by gel permeation chromatography (GPC). Table 1 summarizes some properties of the obtained five P(TMSPMA-*co*-OEGMA) copolymers.

Table 1. OEGMA Contents, Number-Averaged Molecular Weights, and Polydispersity Indices of the Obtained Five P(TMSPMA-*co*-OEGMA) Copolymers

sample code	molar ratio of TMSPMA to OEGMA[a]	M_n ($\times 10^{-4}$) g/mol	PDI
PTO-1	10: 1.0	1.3	1.76
PTO-2	10: 1.8	1.5	2.12
PTO-3	10: 4.4	1.5	2.60
PTO-4	10: 5.9	2.5	2.06
PTO-5	1.0: 10	1.9	1.52

[a]Determined from the ^{1}H NMR spectra of P(TMSPMA-*co*-OEGMA) copolymers.

2.3. Synthesis of Poly[3-(trimethoxysilyl)propyl methacrylate-*co*-4-vinylbenzyl chloride] (P(TMSPMA-*co*-VBC)) Copolymer. The copolymer poly[3-(trimethoxysilyl)propyl methacrylate-*co*-4-vinylbenzyl chloride] (P(TMSPMA-*co*-VBC)) was also synthesized by free radical copolymerization of TMSPMA and VBC. Supporting Information Figure S2 shows the ^{1}H NMR spectrum of the obtained P(TMSPMA-*co*-VBC). The molar ratio of TMSPMA to VBC was determined to be 12: 1 from the ^{1}H NMR spectrum. The number-average molecular weight (M_n) and the polydispersity index (PDI = M_w/M_n) of P(TMSPMA-*co*-VBC) copolymer were measured by GPC to be ~1.66 × 10^4 and 4.9, respectively.

2.4. Fabrication of P(TMSPMA-*co*-OEGMA) and P(TMSPMA-*co*-VBC) Nanocapsules. In a typical preparation of cross-linked P(TMSPMA-*co*-OEGMA) nanocapsules, given amounts of linear cross-linkable copolymer P(TMSPMA-*co*-OEGMA), that is, PTO-1, PTO-2, PTO-3, PTO-4, and PTO-5, were first completely dissolved in 100 μL of toluene, respectively. The P(TMSPMA-*co*-OEGMA) toluene solution was then added into 10 mL of deionized water with a dropwise manner in 1 min under vigorous magnetic stirring, forming an oil-in-water emulsion. Afterward, 10 μL of trimethylamine (TEA) was added into the emulsion to accelerate the hydrolysis and condensation of methoxysilyl groups of P(TMSPMA-*co*-OEGMA). The reaction was allowed to perform at 25 °C under vigorous magnetic stirring (1200 rpm) for 48 h. When the reaction was finished, the reaction mixture was immediately purified by centrifugations and washed with ethanol and deionized water for several times. Scheme 1 shows the hydrolysis and condensation reactions of methoxysilyl groups of P(TMSPMA-*co*-OEGMA) in the presence of the catalyst (TEA) in aqueous solution. Similar procedure was applied to fabricate the cross-linked P(TMSPMA-*co*-VBC) nanocapsules.

2.5. Testing the Polarities of P(TMSPMA-*co*-OEGMA) Nanocapsules in PBS Buffer Solutions (pH = 7.4). A stock solution of pyrene (6 × 10^{-5} M) was made by dissolving pyrene in acetone. Given amounts of pyrene stock solution (10 μL) were dropped into a series of empty vials, which were then allowed to evaporate the acetone and dry overnight in a vacuum oven. The solutions of PTO-1, PTO-2, PTO-3, and PTO-4 nanocapsules were diluted with PBS buffer solutions (pH = 7.4), respectively, to give a series of solutions with various concentration ranging from 0.10 mg/mL down to 1.0 × 10^{-7} mg/mL. Afterward, 1.0 mL of each diluted solution of nanocapsules were transferred to a dried vial containing pyrene, which was allowed to equilibrate for 24 h at room temperature. The final concentration of pyrene in all solutions was 6 × 10^{-7} M, which was less than the pyrene saturation concentration in water. The fluorescence spectra of the nanocapsule buffer solutions were then measured on a LS55 Fluorescence Spectrometer. The intensity ratio (I_1/I_3) of the I_1 (372 nm) and I_3 (383 nm) vibration peaks of the fluorescence spectrum was used to determine the polarity of the pyrene microenvironment, which presented the polarity of the P(TMSPMA-*co*-OEGMA) nanocapsules.

2.6. Preparation of Pyrene-Loaded P(TMSPMA-*co*-OEGMA) Nanocapsules and the Release Behaviors of the Pyrene-Loaded Nanocapsules. Pyrene could be in situ loaded into the P(TMSPMA-*co*-OEGMA) nanocapsules by directly dissolving pyrene in the toluene solution of linear P(TMSPMA-*co*-OEGMA) copolymers before the fabrication of nanocapsules. The concentrations of pyrene in the toluene solutions of PTO-1, PTO-2, PTO-3, and PTO-4 copolymers were the same and 1 × 10^{-3} M. The resultant P(TMSPMA-*co*-OEGMA) nanocapsules containing pyrene were washed with deionized water for several times and collected by centrifugation, which were then dried under vacuum oven at 30 °C for 24 h. The release experiments of pyrene loaded in P(TMSPMA-*co*-OEGMA) nanocapsules were performed in toluene. The time-dependent release of pyrene from the nanocapsules was studied for 360 min. At various release times, the supernatants were collected by centrifuging the nanocapsules and measured with a UV−vis spectrometer. The concentrations of pyrene released from the nanocapsules into toluene were calculated from the adsorption intensities at 338 nm.

2.7. Characterization. ^{1}H NMR spectra of P(TMSPMA-*co*-OEGMA) and P(TMSPMA-*co*-VBC) copolymers were recorded on a 300 MHz Varian Mercury Plus NMR instrument with $CDCl_3$ as solvent. Gel permeation chromatography (GPC) was used to determine molecular weight and molecular weight distribution of the copolymers. GPC measurements were performed on a PL-GPC 220 (Polymer Laboratories, Ltd.) with tetrahydrofuran as the eluent and monodisperse polystyrene as the calibration standard.

The hydrodynamic diameters of the nanocapsules at 25 °C in aqueous solutions or PBS buffer solutions (pH = 7.4) were measured by using dynamic light scattering (DLS) on a Zeta Plus particle size analyzer (Brookhaven Instruments Corp.). The corresponding Zeta potentials of the nanocapsules were measured by electrophoretic light scattering (ELS) using the same Zeta Plus particle size analyzer. Five runs of measurements with each of one minute were performed for each sample as otherwise stated.

Transmission electron microscopy (TEM) measurements were performed on a JEOL JEM-1200 electron microscope operating at an acceleration voltage of 60 KV. The TEM samples were prepared on carbon-coated copper grids, which were immersed in the corresponding sample solutions for a few seconds. The solvent on the copper grids were then gently absorbed away by a filter paper. The copper grids were then allowed to dry in air at room temperature for several hours before observation.

Scanning electron microscopy (SEM) measurements were performed on a Hitachi S4800 electron microscope. The SEM samples were prepared by casting a droplet of the corresponding sample solutions onto the aluminum foils at room temperature. The aluminum foils were allowed to dry in air at room temperature. The samples were coated with platinum vapors before SEM observation.

Fluorescence spectra were recorded on a LS55 Fluorescence Spectrometer (Perkin-Elmer Inc.). Samples were excited at 335 nm with using a 10 nm slit width. Emission wavelengths were scanned from 350 to 500 nm with a 10 nm slit width.

UV−vis spectra were performed on a Cary 300 instrument (Varian Australia Pty Ltd.). The concentrations of pyrene in the toluene solutions were determined from the adsorption intensities at 338 nm.

3. RESULTS AND DISCUSSION

Figures 1 and 2 show the typical TEM and SEM morphologies of the obtained PTO-1 and PTO-3 nanocapsules, which were fabricated from the linear P(TMSPMA-*co*-OEGMA) copoly-

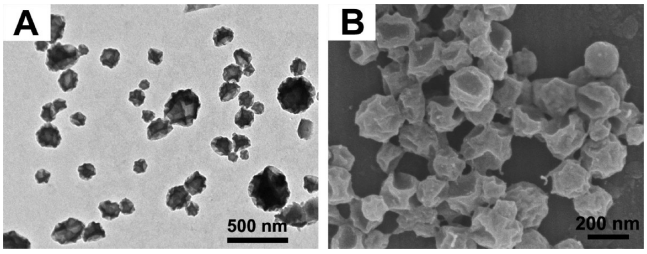

Figure 1. (A) TEM and (B) SEM morphologies of the PTO-1 nanocapsules. The concentration of PTO-1 toluene solution was 0.1 g/mL.

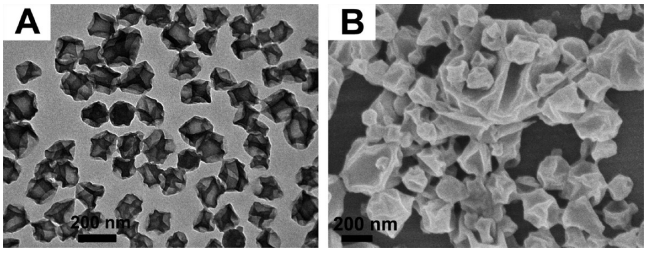

Figure 2. (A) TEM and (B) SEM morphologies of the PTO-3 nanocapsules. The concentration of PTO-3 toluene solution was 0.1 g/mL.

mers, PTO-1 and PTO-3, respectively, with the methods described in the Experimental Section. The typical TEM and SEM morphologies of the obtained PTO-2 and PTO-4 nanocapsules are shown in Figures S3 and S4 (see Supporting Information). Clearly, P(TMSPMA-*co*-OEGMA) nanocapsules were successfully obtained. The formation mechanism of P(TMSPMA-*co*-OEGMA) nanocapsules is similar with that reported previously for PTMSPMA nanocapsules.[23] Briefly, the oil-in-water emulsion was formed with toluene droplets containing cross-linkable copolymer P(TMSPMA-*co*-OEGMA) in the continuous water phase. In this case, the hydrophilic character of OEGMA will make the copolymer P(TMSPMA-*co*-OEGMA) prefer to locate at the interfaces of the toluene droplets and continuous water phase. The hydrolysis and condensation of methoxysilyl groups further resulted in the internal phase separation of P(TMSPMA-*co*-OEGMA) within the toluene droplets and led the cross-linked P(TMSPMA-*co*-OEGMA) migrate to the toluene/water interfaces, forming an interfacial cross-linked P(TMSPMA-*co*-OEGMA) layer. Finally, the completion of hydrolysis and condensation of methoxysilyl groups led to the formation of robustly cross-linked P(TMSPMA-*co*-OEGMA) shells, that is, the P(TMSPMA-*co*-OEGMA) nanocapsules. Scheme 2 shows the possible structure of the P(TMSPMA-*co*-OEGMA) nanocapsule. The oligo(ethylene glycol) (OEG) moieties tended to point into the water phase in the mixing solution and hence locate at the surfaces of the resultant nanocapsules because of the hydrophilic character of OEG. The morphologies of PTO-1, PTO-2, PTO-3, and PTO-4 nanocapsules obtained here could be assigned to multifold morphologies according to the previous classification.[23] The diameters of nanocapsules in the TEM images were then calculated by measuring the two farthest points of the nanocapsules as shown in Supporting Information Figure S5, which would be the closest value for the size of the dried nanocapsules. The average diameters of PTO-1, PTO-2, PTO-3, and PTO-4 nanocapsules obtained by TEM images were 280 ± 95, 182 ± 72, 158 ± 45, and 192 ± 78 nm,

Scheme 2. Schematic Illustration of Structure of P(TMSPMA-*co*-OEGMA) Nanocapsule

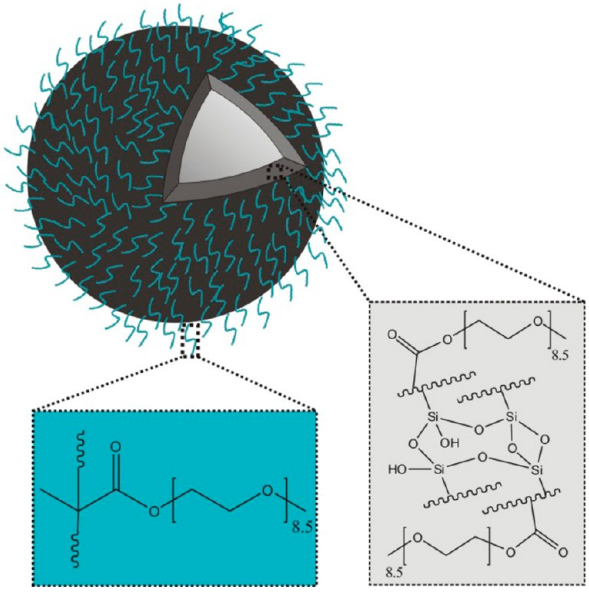

respectively. The morphologies of nanocapsules could be classified as three main hollow structures of classic hollow morphologies, Kippah morphologies, and multifold morphologies. The large nanocapsules with sizes >∼100 nm were prone to collapse and form the multifold morphologies.[23] The wall thickness of nanocapsules could be estimated by measuring the size of the folds observed in the TEM image as indicated in Supporting Information Figure S5. Note that the apparent wall thicknesses of nanocapsules with multifold morphologies from their TEM images were approximately double their actual wall thickness value.[23] At least 100 nanocapsules from the TEM images were measured for calculating the average diameter and wall thickness of the nanocapsules. The wall thicknesses of PTO-1, PTO-2, PTO-3, and PTO-4 nanocapsules were then estimated to be approximately 8, 10, 9, and 9 nm, respectively. It can be also seen from the TEM images that the obtained P(TMSPMA-*co*-OEGMA) nanocapsules exhibited large size distributions, as shown in Supporting Information Figure S6.

However, for the copolymer PTO-5 with highest OEGMA content, that is, the molar ratio of TMSPMA to OEGMA was 1.0:10, only irregular nanoparticles were obtained, as shown in Figure 3. There were two possible reasons for such phenomena. One was that the copolymer PTO-5 was "*too*" hydrophilic because of the large percent of OEGMA so that it was impossible to maintain the spherical shells. As a result, the

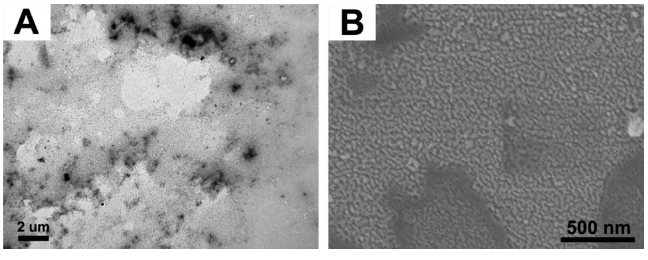

Figure 3. (A) TEM and (B) SEM morphologies of the PTO-5 nanocapsules. The concentration of PTO-5 toluene solution was 0.1 g/mL.

PTO-5 might mainly participate in the continuous water phase so that the partition fraction of the PTO-5 in the toluene droplet was less enough to form the interfacial layer, which was necessary for the formation of nanocapsule. Small micelles or aggregates with hydrophobic PTMSPMA segments as cores and hydrophilic OEGMA segments as coronas might be formed when mixing PTO-5 toluene solutions with large amount of deionized water. The other reason was that the amount of cross-linkable TMSPMA segments was not enough to keep the shapes of cross-linked structures. The structures formed in the PTO-5 mixing solution were only weak cross-linked, resulting in the irregular shapes. These results suggested that there was a critical threshold of OEGMA content for the successful fabrication of P(TMSPMA-*co*-OEGMA) nanocapsules. The present works indicated that P(TMSPMA-*co*-OEGMA) nanocapsules could be successfully obtained from P(TMSPMA-*co*-OEGMA) copolymer with the molar ratio of TMSPMA to OEGMA $\geq$ 1.7 studied here.

The hydrodynamic diameters of PTO-1, PTO-2, PTO-3, and PTO-4 nanocapsules in deionized water and PBS buffer solutions (pH =7.4) were measured by dynamic light scattering, respectively, as shown in Figure 4. The DLS results clearly

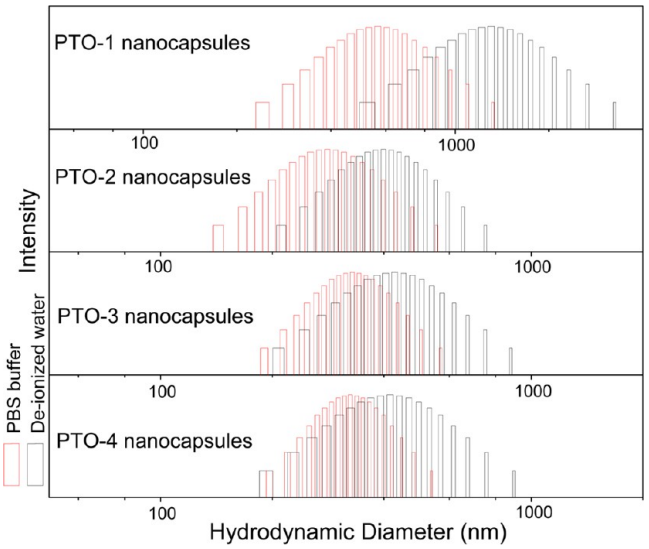

Figure 4. Distributions of hydrodynamic diameters of PTO-1, PTO-2, PTO-3, and PTO-4 nanocapsules in deionized water (black columns) and PBS buffer solutions (pH =7.4, red columns) obtained by dynamic light scattering (DLS) measurements.

showed that the obtained P(TMSPMA-*co*-OEGMA) nanocapsules had large size distributions, which were consistent with those obtained by TEM observations. Interestingly, the size distribution of the P(TMSPMA-*co*-OEGMA) nanocapsules in PBS buffer solutions (pH = 7.4) became narrow as comparing with those in deionized water. The hydrodynamic diameters of the P(TMSPMA-*co*-OEGMA) nanocapsules also shifted to the lower values in PBS buffer solutions (pH= 7.4). These results were understandable because the P(TMSPMA-*co*-OEGMA) nanocapsules had larger swelling extent in the deionized water than that in PBS buffer solution because of the hydrophilic nature of OEGMA segments and larger surface charge densities (or Zeta potentials) of the nanocapsules in deionized water (see below). Because the PBS buffer solution also contains salts, the influences of adding salt on the size and size distribution of the P(TMSPMA-*co*-OEGMA) nanocapsules were also tested. Note that the salt concentration of PBS buffer solution was ~0.01 M and the main component of PBS buffer solution was sodium chloride, that is, NaCl. NaCl was thus used to check the influence of adding salt on the size and the size distribution of P(TMSPMA-*co*-OEGMA) nanocapsules. The salt concentration of 0.01 M NaCl was obtained by in situ adding given amounts of 0.03 M NaCl aqueous solution into the nanocapsules aqueous dispersion. The size and size distribution of the P(TMSPMA-*co*-OEGMA) nanocapsules with 0.01 M NaCl were immediately measured by DLS. DLS measurements indicated that the size change of the nanocapsules occurred in less than 30 s. Note that the data acquisition times for DLS measurements here were set to be 30 s. DLS measurements also indicated that the hydrodynamic diameters of the P(TMSPMA-*co*-OEGMA) nanocapsules shifted to the higher values in 0.01 M NaCl aqueous solution and the size distribution of the P(TMSPMA-*co*-OEGMA) nanocapsules in 0.01 M NaCl aqueous solution became broader as comparing with those in deionized water without salt, as shown in Supporting Information Figure S7. However, the results of Figure 4 clearly indicated that the size distribution of the P(TMSPMA-*co*-OEGMA) nanocapsules in PBS buffer solutions (pH = 7.4) became narrow as comparing with those in deionized water and the hydrodynamic diameters of the P(TMSPMA-*co*-OEGMA) nanocapsules also shifted to the lower values in PBS buffer solutions (pH = 7.4). These results further suggested that the changes of size and size distribution of the P(TMSPMA-*co*-OEGMA) nanocapsules in PBS buffer solution were not due to the osmosis effects with the presence of salts.

Figure 5 shows the surface charge densities, measured as Zeta potentials, of PTO-1, PTO-2, PTO-3, and PTO-4 nanocapsules

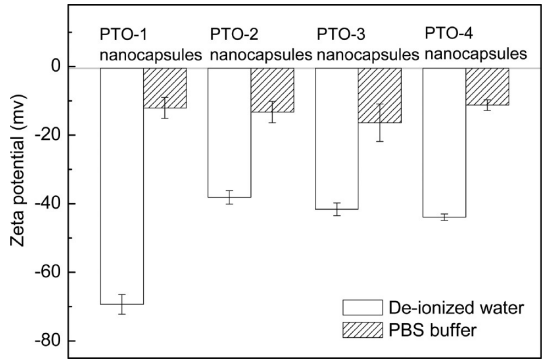

Figure 5. Zeta potentials of PTO-1, PTO-2, PTO-3, and PTO-4 nanocapsules in deionized water (empty columns) and PBS buffer (pH = 7.4, filled columns) solutions.

in deionized water and PBS buffer solutions, respectively. All nanocapsules were negatively charged in deionized water and PBS buffer solutions (pH = 7.4). It was reasonable because the hydrolysis of methoxysilyl groups gave silanol groups (Si−OH), which will be negatively charged. The Zeta potentials of PTO-1, PTO-2, PTO-3, and PTO-4 nanocapsules were −69.3, −38.1, −41.6, and −43.9 mV in deionized water, respectively. There was not clear relationship between the Zeta potentials and the OEGMA or TMSPMA contents of the nanocapsules. In the PBS buffer solutions (pH = 7.4), the PTO-1, PTO-2, PTO-3, and PTO-4 nanocapsules were also negatively charged with Zeta potentials of −12.0, −13.3, −16.4, and −11.3 mV, respectively, which were much smaller than those measured in

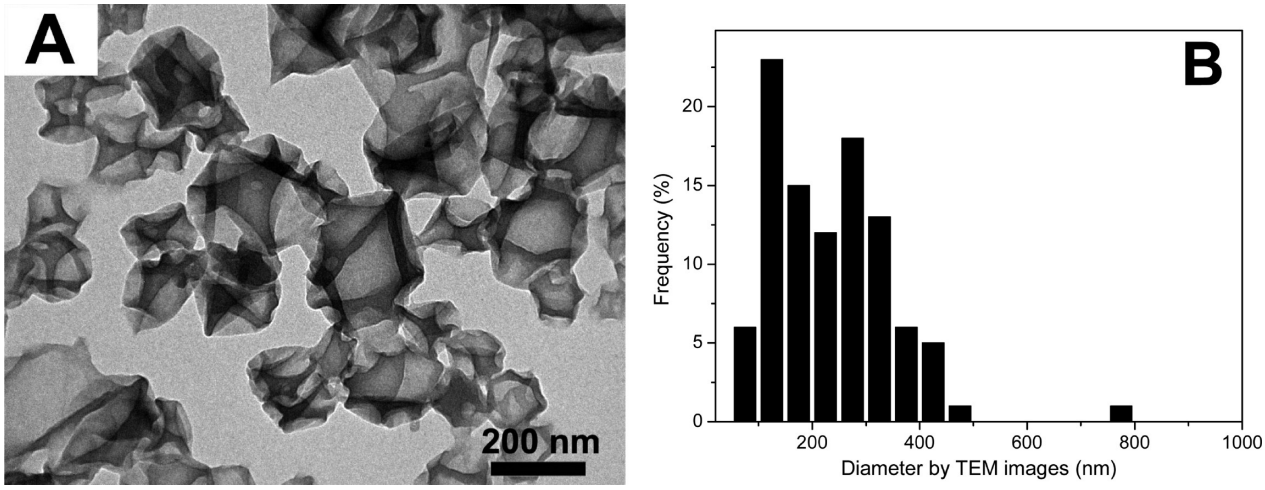

Figure 6. (A) TEM morphologies and (B) size distribution of the PTO-3−05 nanocapsules prepared from the PTO-3 toluene solution with concentration of 0.05 g/mL.

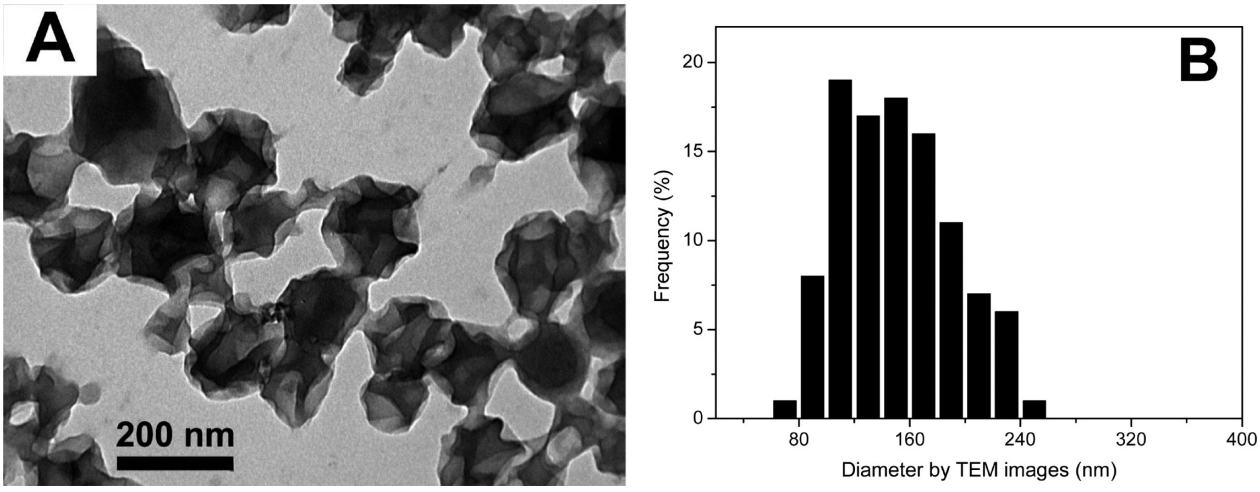

Figure 7. (A) TEM morphologies and (B) size distribution of the PTO-3−2 nanocapsules prepared from the PTO-3 toluene solution with concentration of 0.2 g/mL.

deionized water. Increasing the contents of OEGMA of the copolymer P(TMSPMA-*co*-OEGMA) will increase the OEG densities on the surfaces of the resultant nanocapsules. However, the influence of surface OEG densities on the surface charge densities of the P(TMSPMA-*co*-OEGMA) nanocapsules was almost negligible in PBS buffer solutions. It was common for polymer nanoparticles with PEG-functionalized surfaces that the Zeta potentials of such polymer nanoparticles would have higher Zeta potentials in deionized water than those in PBS buffer solutions.[40,41] Graf et al.[40] reported that the Zeta potential of silica nanoparticles with PEG-functionalized surfaces was −49 mV in deionized water (pH = 6.5), which was higher than that of +6 mV in PBS buffer solution (pH = 7.4). Recently, Zhang et al.[41] also reported that the Zeta potential of micelles with PEG surfaces was −18.0 mV in PBS buffer solution (pH = 5.0) and −12.2 mV in PBS buffer solution (pH = 7.4), respectively.

The influences of copolymer concentrations on the sizes and wall thicknesses of P(TMSPMA-*co*-OEGMA) nanocapsules were also investigated. Figures 6 and 7 show the TEM morphologies and size distributions of P(TMSPMA-*co*-OEGMA) PTO-3−05 and PTO-3−2 nanocapsules, which were prepared from the PTO-3 toluene solutions with concentrations of 0.05 and 0.2 g/mL, respectively. As compared with the results shown in Figure 2, the average sizes of PTO-3 nanocapsules fabricated from the PTO-3 toluene solutions with concentrations of 0.05, 0.1, and 0.2 g/mL were 235 ± 113, 158 ± 45, and 150 ± 40 nm, respectively, as measured by TEM. The hydrodynamic diameter and SEM images of PTO-3−05 and PTO-3−2 nanocapsules are shown in Supporting Information Figures S8 and S9, respectively. These results might indicate that the average sizes of P(TMSPMA-*co*-OEGMA) nanocapsules decreased with increasing the concentration of copolymer. Similarly, the PTO-3−05 and PTO-3−2 nanocapsules were collapsed to form multifold morphologies with the wall thicknesses of approximately 12 and 10 nm, respectively.

The relationship of the wall thickness, copolymer concentration and the radius of the nanocapsule could be given as

$$t = r\left(1 - \sqrt[3]{1 - \frac{(1-f)c_p}{\rho_s}}\right) \quad (1)$$

where f is the loss factor, which was the factor of the lose mass of P(TMSPMA-*co*-OEGMA) copolymer during the hydrolysis

dx.doi.org/10.1021/am400365s | ACS Appl. Mater. Interfaces 2013, 5, 3748−3756

and condensation reactions; ρ_s is the density of shell in the dried state without any solvent; c_p is the concentration of the copolymer droplet; t is the wall thickness of the shell; r is the radius of the nanocapsule. The derivation of eq 1 was given in the Supporting Information. According to the eq 1, it could be found that the wall thickness was influenced by many factors, including the radius of the nanocapsules, the concentration of the copolymer, the density of the wall, and the loss factor. For example, the concentration of PTO-3 copolymer for the fabrication of PTO-3−05 nanocapsules was half of the PTO-3 nanocapsules, but the wall thickness of PTO-3−05 nanocapsules, i.e. ca. 12 nm was larger than that of PTO-3 nanocapsules, that is, ∼9 nm. The reason was that the diameter of PTO-3−05 nanocapsules was much larger than that of PTO-3 nanocapsules. The diameters of nanocapsules played an important role in determining their wall thickness. It was worthy to note that the wall thickness was an average value of many nanocapsules so that the size distribution of nanocapsules was also very important. Although we were currently not able to control the wall thickness of the obtained P(TMSPMA-*co*-OEGMA) nanocapsules, an important conclusion might be drawn here: it was crucial and necessary to fabricate polymer nanocapsules with monodisperse size distribution so that the wall thickness of the nanocapsules could be then controlled. Recently, Tissot et al.[42] reported that the thickness of shell of monodispersed hollow silica nanoparticles should also be dependent on the diameter of the monodispersed polymer beads.

Since the polymer nanocapsules had great potential applications as drug delivery systems, it was important to know the polarities of the obtained P(TMSPMA-*co*-OEGMA) nanocapsules, which would be helpful for determining whether the hydrophobic or hydrophilic drugs could be loaded into the nanocapsules. The polarities of PTO-1, PTO-2, PTO-3, and PTO-4 nanocapsules in PBS buffer solutions were then investigated by using pyrene as probe. Pyrene is known as molecular indicator for detecting the polarity of the microenvironment.[43−47] The intensity ratio (I_1/I_3) of the first peak (I_1 = 372 nm) to the third peak (I_3 = 383 nm) of the fluorescence emission spectrum of pyrene is sensitive to the polarity of the microenvironment where pyrene molecules located.[44,47] Pyrene is poorly soluble in water, and the intensity ratio (I_1/I_3) is 1.6 in PBS buffer solutions.[47] However, it strongly emits radiation when it locates in a hydrophobic microenvironment and the intensity ratio (I_1/I_3) becomes much lower.[44,47] Hence, pyrene has been widely used in many fields, such as the determination of critical micelle concentration (CMC)[44] and the polarities of environments of nanospheres with different temperatures.[46] Recently, Liu et al. reported that the I_1/I_3 ratio in an aqueous suspension of the magnetic/thermally sensitive nanospheres (F127-MNPs) varies from 0.8 to 0.2 with the increasing of temperature.[46] This result meant that the F127-MNPs were more hydrophobic above 25 °C, as the pyrene partition changed to a more hydrophobic environment as the micellar aggregation began to form. Figure 8 shows the I_1/I_3 ratios of pyrene as a function of the concentrations of PTO-1, PTO-2, PTO-3, and PTO-4 nanocapsules in PBS buffer solutions (pH = 7.4). The I_1/I_3 ratios of pyrene in PBS buffer solutions with P(TMSPMA-*co*-OEGMA) nanocapsules were ∼0.80−1.05, which were lower than that in pure PBS buffer solution (I_1/I_3 = 1.6).[47] It indicated that the pyrene molecules entered into the P(TMSPMA-*co*-OEGMA) nanocapsules even with a very low

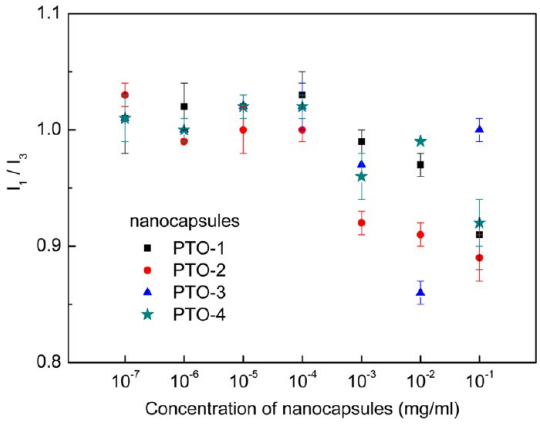

Figure 8. I_1/I_3 ratios of pyrene as a function of the concentrations of PTO-1, PTO-2, PTO-3, and PTO-4 nanocapsules in PBS buffer solutions (pH = 7.4).

concentration of 10^{-7} mg/mL. These results strongly suggested that the microenvironments of P(TMSPMA-*co*-OEGMA) nanocapsules were hydrophobic. It was reasonable because TMSPMA was hydrophobic in nature and the cross-linked walls of the nanocapsules mainly consisted of cross-linked poly(TMSPMA) segments. The pyrene molecules tended to adsorb and locate at the hydrophobic walls of the nanocapsules, leading to the low values of I_1/I_3 ratios. Furthermore, the data of Figure 8 also showed that the I_1/I_3 ratios of pyrene were similar for PTO-1, PTO-2, PTO-3, and PTO-4 nanocapsules with various concentrations, indicating that the hydrophobic properties of the cross-linked walls of the four P(TMSPMA-co-OEGMA) nanocapsules were similar regardless of the contents of OEGMA studied here. Although the contents of OEGMA did not affect the polarity of microenvironments of the obtained P(TMSPMA-*co*-OEGMA) nanocapsules, it was found that the contents of OEGMA did affect the permeation properties of the resultant P(TMSPMA-*co*-OEGMA) nanocapsules.

Since the microenvironments of P(TMSPMA-*co*-OEGMA) nanocapsules were hydrophobic, hydrophobic drugs might be loaded into the nanocapsules. Here, pyrene was selected as the model drug to be loaded into the P(TMSPMA-*co*-OEGMA) nanocapsules and the release behavior of pyrene from the nanocapsules into the toluene was then investigated. By simply fabricating the P(TMSPMA-*co*-OEGMA) nanocapsules from the toluene solution of linear copolymer P(TMSPMA-*co*-OEGMA) containing given amounts of pyrene, one could have pyrene in situ loaded into the resultant P(TMSPMA-*co*-OEGMA) nanocapsules. After the formation of cross-linked P(TMSPMA-*co*-OEGMA) shells, the hydrophobic molecules, which were within the toluene droplets, that is, pyrene, were confined inside the nanocapsules. Supporting Information Figure S11 shows the presented UV−vis spectrum of PTO-2 nanocapsules loaded with pyrene in deionized water. Characteristic absorption bands of pyrene at 260, 267, 274, and 338 nm were clearly observed, indicating the successful loading of pyrene into the P(TMSPMA-*co*-OEGMA) nanocapsules. Four P(TMSPMA-*co*-OEGMA) nanocapsules with in situ loaded pyrene were then successful prepared, that is, PTO-1, PTO-2, PTO-3, and PTO-4 nanocapsules, as described in the Experimental Section. The release behaviors of loaded pyrene from these nanocapsules into toluene were studied, as shown Figure 9. The release percentages of pyrene from the pyrene-

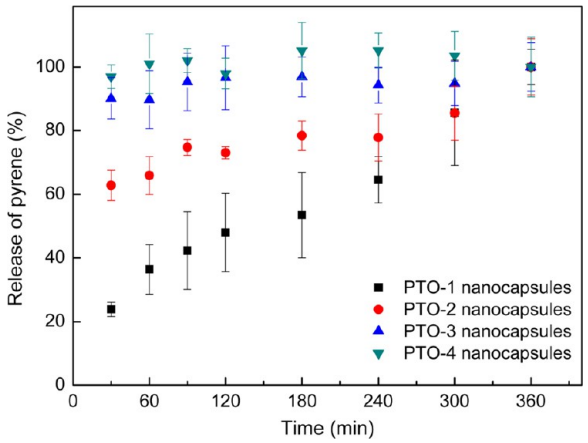

Figure 9. Release profiles of pyrene from the PTO-1, PTO-2, PTO-3, and PTO-4 nanocapsules into toluene as a function of times.

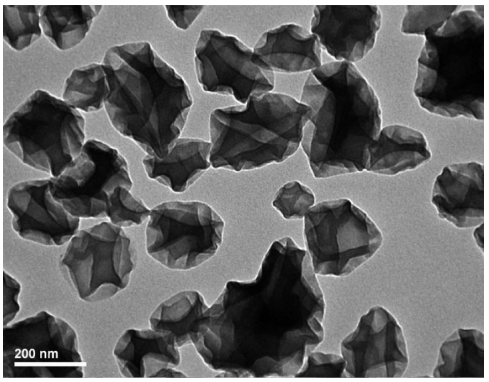

Figure 10. TEM image of the cross-linked P(TMSPMA-*co*-VBC) nanocapsules fabricated with the toluene solution of P(TMSPMA-*co*-VBC) of 0.1 g/mL at 25 °C.

loaded PTO-1, PTO-2, PTO-3, and PTO-4 nanocapsules into toluene at testing release times of 30 min were PTO-1 < PTO-2 < PTO-3 < PTO-4. These results indicated that increasing the OEGMA contents of P(TMSPMA-co-OEGMA) nanocapsules increased the release percentage of pyrene. Especially, for PTO-4 nanocapsules, pyrene was almost completely released out from the nanocapsules into toluene within 30 min. The release rate of pyrene increased with increasing the contents of OEGMA, that is, PTO-1 < PTO-2 < PTO-3 < PTO-4. In other word, the permeation properties of the P(TMSPMA-*co*-OEGMA) nanocapsules for pyrene were strongly dependent on the content of OEGMA. The increase of OEGMA fraction, i.e. the decrease of TMSPMA fraction, led to the decrease of cross-linked density of the walls of the resultant P(TMSPMA-*co*-OEGMA) nanocapsules. The walls of nanocapsules with lower cross-linked densities will then have higher permeation properties. These results suggested that it was able to tune the permeation properties of polymer nanocapsules by controlling the cross-linked densities of the nanocapsule walls.

The above results clearly showed that P(TMSPMA-*co*-OEGMA) nanocapsules with controllable OEG densities and permeation properties could be obtained from the linear copolymers P(TMSPMA-*co*-OEGMA) with various OEGMA contents. Such method could be also applied to incorporate other functional groups into the polymer nanocapsules. Another linear copolymer, poly[3-(trimethoxysilyl)propyl methacrylate-*co*-4-vinylbenzyl chloride] (P(TMSPMA-*co*-VBC)), was then synthesized to demonstrate the incorporation of VBC into the resultant polymer nanocapsules. The molar ratio of TMSPMA to VBC was 12: 1 as calculated by ^{1}H NMR spectrum (Supporting Information Figure S2). The number-average molecular weight (M_n) and the polydispersity index (PDI = M_w/M_n) of P(TMSPMA-*co*-VBC) copolymer were 1.66 × 10^4 and 4.9, respectively. Note that OEGMA is a hydrophilic monomer and biocompatible, but 4-vinylbenzyl chloride (VBC) is a hydrophobic monomer and could be used for further modification due to the easy and versatile functionalization of its chloromethyl group.[48] Figure 10 shows the TEM morphologies of P(TMSPMA-*co*-VBC) nanocapsules. The average diameter of P(TMSPMA-*co*-VBC) nanocapsules was calculated to be ~303 ± 109 nm. The successful fabrication of P(TMSPMA-*co*-VBC) nanocapsules indicated that various functional groups could be introduced into the resultant polymer nanocapsules by using such methodology. The preparation of polymer nanocapsules with various functionalities and robustly cross-linked walls without any further post modification process, any sacrificial core and surfactant would be beneficial from scientific and technical point of views.

4. CONCLUSIONS

P(TMSPMA-*co*-OEGMA) nanocapsules with controllable oligo(ethylene glycol) (OEG) densities and permeation properties, as well as robustly cross-linked walls were successfully fabricated from the cross-linkable copolymer, poly[3-(trimethoxysilyl)propyl methacrylate-*co*-oligo(ethylene glycol) methacrylate] (P(TMSPMA-*co*-OEGMA)). The densities of OEG segments of the resultant P(TMSPMA-*co*-OEGMA) nanocapsules could be easily controlled by tuning the OEGMA contents of copolymer P(TMSPMA-*co*-OEGMA), which would not be affected during the fabrication process of polymer nanocapsules. The microenvironments of the obtained P(TMSPMA-*co*-OEGMA) nanocapsules were hydrophobic. It was confirmed that the hydrophobic pyrene could be in situ loaded into the P(TMSPMA-*co*-OEGMA) nanocapsules during the fabrication procedures. The release rates of pyrene from the P(TMSPMA-*co*-OEGMA) nanocapsules were dependent on the contents of OEGMA, indicating that the permeation properties of P(TMSPMA-*co*-OEGMA) nanocapsules could be tuned by varying the cross-linked densities of the nanocapsule walls. Such method could be applied to introduce various functional groups into the resultant polymer nanocapsules.

■ ASSOCIATED CONTENT

Supporting Information

^{1}H NMR spectra of P(TMSPMA-*co*-OEGMA) copolymers, ^{1}H NMR spectrum for P(TMSPMA-*co*-VBC) copolymer, TEM and SEM images of the PTO-2 and PTO-4 nanocapsules, size distributions of nanocapsules calculated from their TEM images, distributions of hydrodynamic diameters of nanocapsules in 0.01 M NaCl aqueous solutions, hydrodynamic diameters and SEM morphologies of the PTO-3−05 and PTO-3−2 nanocapsules, the analysis and calculation of the wall thickness of nanocapsule, UV−vis spectrum of pyrene loaded PTO-2 nanocapsules, and hydrodynamic diameters of P(TMSPMA-*co*-VBC) nanocapsules in deionized water measured by DLS and size distribution of P(TMSPMA-*co*-VBC) nanocapsules obtained from their TEM images. This

dx.doi.org/10.1021/am400365s | ACS Appl. Mater. Interfaces 2013, 5, 3748−3756

information is available free of charge via the Internet at http://pubs.acs.org/.

AUTHOR INFORMATION

Corresponding Author

*E-mail: duby@zju.edu.cn.

Notes

The authors declare no competing financial interest.

ACKNOWLEDGMENTS

The authors thank the National Natural Science Foundation of China (Nos. 21074114 and 21274129) for financial supports.

REFERENCES

(1) Kulkamp, I. C.; Rabelo, B. D.; Berlitz, S. J.; Isoppo, M.; Bianchin, M. D.; Schaffazick, S. R.; Pohlmann, A. R.; Guterres, S. S. *J. Biomed. Nanotechnol.* **2011**, *7*, 598−607.
(2) Diaz-Lopez, R.; Tsapis, N.; Santin, M.; Bridal, S. L.; Nicolas, V.; Jaillard, D.; Libong, D.; Chaminade, P.; Marsaud, V.; Vauthier, C.; Fattal, E. *Biomaterials* **2010**, *31*, 1723−1731.
(3) Yan, M.; Du, J.; Gu, Z.; Liang, M.; Hu, Y.; Zhang, W.; Priceman, S.; Wu, L.; Zhou, Z. H.; Liu, Z.; Segura, T.; Tang, Y.; Lu, Y. *Nat. Nanotechnol.* **2010**, *5*, 48−53.
(4) Yan, M.; Liang, M.; Wen, J.; Liu, Y.; Lu, Y.; Chen, I. S. Y. *J. Am. Chem. Soc.* **2012**, *134*, 13542−13545.
(5) Mandal, S. K.; Dutta, P. *J. Nanosci. Nanotechnol.* **2004**, *4*, 972−975.
(6) An, K.; Hyeon, T. *Nano Today* **2009**, *4*, 359−373.
(7) Zhao, Y.; Jiang, L. *Adv. Mater.* **2009**, *21*, 3621−3638.
(8) Son, K. J.; Yoon, H.-J.; Kim, J.-H.; Jang, W.-D.; Lee, Y.; Koh, W.-G. *Angew. Chem., Int. Ed.* **2011**, *50*, 11968−11971.
(9) Caruso, F.; Trau, D.; Mohwald, H.; Renneberg, R. *Langmuir* **2000**, *16*, 1485−1488.
(10) Donath, E.; Sukhorukov, G. B.; Caruso, F.; Davis, S. A.; Möhwald, H. *Angew. Chem., Int. Ed.* **1998**, *37*, 2201−2205.
(11) Such, G. K.; Quinn, J. F.; Quinn, A.; Tjipto, E.; Caruso, F. *J. Am. Chem. Soc.* **2006**, *128*, 9318−9319.
(12) Ma, G.-H.; Sone, H.; Omi, S. *Macromolecules* **2004**, *37*, 2954−2964.
(13) Yu, X.; Zhao, Z.; Nie, W.; Deng, R.; Liu, S.; Liang, R.; Zhu, J.; Ji, X. *Langmuir* **2011**, *27*, 10265−10273.
(14) Zhang, J.; Ge, X.; Wang, M.; Yang, J.; Wu, Q.; Wu, M.; Liu, N.; Jin, Z. *Chem. Commun.* **2010**, *46*, 4318−4320.
(15) Yow, H. N.; Routh, A. F. *Soft Matter* **2006**, *2*, 940−949.
(16) Jang, J.; Lee, K. *Chem. Commun.* **2002**, *38*, 1098−1099.
(17) Zha, L. S.; Zhang, Y.; Yang, W. L.; Fu, S. K. *Adv. Mater.* **2002**, *14*, 1090−1092.
(18) Du, J. Z.; Chen, Y. M. *Macromolecules* **2004**, *37*, 5710−5716.
(19) Du, J. Z.; Chen, Y. M.; Zhang, Y. H.; Han, C. C.; Fischer, K.; Schmidt, M. *J. Am. Chem. Soc.* **2003**, *125*, 14710−14711.
(20) Danila, D. C.; Banner, L. T.; Karimova, E. J.; Tsurkan, L.; Wang, X.; Pinkhassik, E. *Angew. Chem., Int. Ed.* **2008**, *47*, 7036−7039.
(21) Dergunov, S. A.; Kesterson, K.; Li, W.; Wang, Z.; Pinkhassik, E. *Macromolecules* **2010**, *43*, 7785−7792.
(22) Gomes, J. F. P. d. S.; Sonnen, A. F. P.; Kronenberger, A.; Fritz, J.; Coelho, M. Á. N.; Fournier, D.; Fournier-Nöel, C.; Mauzac, M.; Winterhalter, M. *Langmuir* **2006**, *22*, 7755−7759.
(23) Chen, T.; Du, B.; Fan, Z. *Langmuir* **2012**, *28*, 11225−11231.
(24) Cao, Z.; Du, B.; Chen, T.; Nie, J.; Xu, J.; Fan, Z. *Langmuir* **2008**, *24*, 12771−12778.
(25) Yuan, J.; Xu, Y.; Walther, A.; Bolisetty, S.; Schumacher, M.; Schmalz, H.; Ballauff, M.; Muller, A. H. E. *Nat. Mater.* **2008**, *7*, 718−722.
(26) Du, B. Y.; Mei, A. X.; Tao, P. J.; Zhao, B.; Cao, Z.; Nie, J. J.; Xu, J. T.; Fan, Z. Q. *J. Phys. Chem. C* **2009**, *113*, 10090−10096.
(27) Mullner, M.; Yuan, J. Y.; Weiss, S.; Walther, A.; Fortsch, M.; Drechsler, M.; Muller, A. H. E. *J. Am. Chem. Soc.* **2010**, *132*, 16587−16592.
(28) Chen, T. Y.; Cao, Z.; Guo, X. L.; Nie, J. J.; Xu, J. T.; Fan, Z. Q.; Du, B. Y. *Polymer* **2011**, *52*, 172−179.
(29) Manson, J.; Kumar, D.; Meenan, B.; Dixon, D. *Gold Bull.* **2011**, *44*, 99−105.
(30) Thierry, B.; Griesser, H. J. *J. Mater. Chem.* **2012**, *22*, 8810−8819.
(31) Wattendorf, U.; Kreft, O.; Textor, M.; Sukhorukov, G. B.; Merkle, H. P. *Biomacromolecules* **2007**, *9*, 100−108.
(32) Baier, G.; Siebert, J. M.; Landfester, K.; Musyanovych, A. *Macromolecules* **2012**, *45*, 3419−3427.
(33) Morral-Ruíz, G.; Solans, C.; García, M. L.; García-Celma, M. J. *Langmuir* **2012**, *28*, 6256−6264.
(34) Rosenbauer, E.-M.; Landfester, K.; Musyanovych, A. *Langmuir* **2009**, *25*, 12084−12091.
(35) Kono, K.; Fukui, T.; Takagishi, T.; Sakurai, S.; Kojima, C. *Polymer* **2008**, *49*, 2832−2838.
(36) Hak, S.; Helgesen, E.; Hektoen, H. H.; Huuse, E. M.; Jarzyna, P. A.; Mulder, W. J. M.; Haraldseth, O.; Davies, C. d. L. *ACS Nano* **2012**, *6*, 5648−5658.
(37) Wagner, V.; Dullaart, A.; Bock, A.-K.; Zweck, A. *Nat. Biotechnol.* **2006**, *24*, 1211−1217.
(38) Sheng, Y.; Yuan, Y.; Liu, C.; Tao, X.; Shan, X.; Xu, F. *J. Mater. Sci.: Mater. Med.* **2009**, *20*, 1881−1891.
(39) Essa, S.; Rabanel, J. M.; Hildgen, P. *Int. J. Pharm.* **2011**, *411*, 178−187.
(40) Graf, C.; Gao, Q.; Schütz, I.; Noufele, C. N.; Ruan, W.; Posselt, U.; Korotianskiy, E.; Nordmeyer, D.; Rancan, F.; Hadam, S.; Vogt, A.; Lademann, J.; Haucke, V.; Rühl, E. *Langmuir* **2012**, *28*, 7598−7613.
(41) Zhang, S.; Zou, J.; Zhang, F.; Elsabahy, M.; Felder, S. E.; Zhu, J.; Pochan, D. J.; Wooley, K. L. *J. Am. Chem. Soc.* **2012**, *134*, 18467−18474.
(42) Tissot, I.; Reymond, J. P.; Lefebvre, F.; Bourgeat-Lami, E. *Chem. Mater.* **2002**, *14*, 1325−1331.
(43) Bromberg, L. E.; Barr, D. P. *Macromolecules* **1999**, *32*, 3649−3657.
(44) Greene, A. C.; Zhu, J.; Pochan, D. J.; Jia, X.; Kiick, K. L. *Macromolecules* **2011**, *44*, 1942−1951.
(45) Kalyanasundaram, K.; Thomas, J. K. *J. Am. Chem. Soc.* **1977**, *99*, 2039−2044.
(46) Liu, T.-Y.; Hu, S.-H.; Liu, K.-H.; Shaiu, R.-S.; Liu, D.-M.; Chen, S.-Y. *Langmuir* **2008**, *24*, 13306−13311.
(47) Wan, D.; Ohta, S.; Kakuchi, T.; Satoh, T. *Soft Matter* **2011**, *7*, 6422−6425.
(48) Hemp, S. T.; Allen, M. H.; Green, M. D.; Long, T. E. *Biomacromolecules* **2012**, *13*, 231−238.